Optical switching at 1.55μm in silicon racetrack resonators using phase change materials

Miquel Rudé, Josselin Pello, Robert E. Simpson, Johann Osmond, Gunther Roelkens et al.

Additional information on Appl. Phys. Lett.

Optical switching at 1.55 μm in silicon racetrack resonators using phase change materials

Miquel Rudé,[1,a)] Josselin Pello,[2] Robert E. Simpson,[3] Johann Osmond,[1] Gunther Roelkens,[4] Jos J. G. M. van der Tol,[2] and Valerio Pruneri[1,5]

[1]ICFO-Institut de Ciències Fotòniques, 08860 Castelldefels, Spain
[2]Eindhoven University of Technology, 5600 MB Eindhoven, The Netherlands
[3]Singapore University of Technology and Design, 138683 Singapore, Singapore
[4]Ghent University - IMEC, 9000 Ghent, Belgium
[5]ICREA-Institució Catalana de Recerca i Estudis Avançats, 08010 Barcelona, Spain

An optical switch operating at a wavelength of 1.55 μm and showing a 12 dB modulation depth is introduced. The device is implemented in a silicon racetrack resonator using an overcladding layer of the phase change data storage material $Ge_2Sb_2Te_5$, which exhibits high contrast in its optical properties upon transitions between its crystalline and amorphous structural phases. These transitions are triggered using a pulsed laser diode at $\lambda = 975$ nm and used to tune the resonant frequency of the resonator and the resultant modulation depth of the 1.55 μm transmitted light. © 2013 AIP Publishing LLC. [http://dx.doi.org/10.1063/1.4824714]

The ever-increasing demand for high speed optical communication networks is driving the development of new photonic devices that can process optical signals in a reliable, low-cost manner. Among competing technologies, Si-based devices have emerged as one of the main candidates for such applications, and several devices, including modulators,[1–5] add-drop filters,[6] and wavelength division multiplexers (WDM)[7] have already been demonstrated. An important branch of this technology is the ability to program reconfigurable optical circuits. Indeed, a reprogrammable optical circuit that can hold its configuration without an external continuous source is extremely desirable for a multitude of applications ranging from photonic routers to optical cognitive networks. Recently, new solutions for non-volatile photonic memories have been proposed, involving the use of phase-change materials (PCMs) and racetrack resonators.[8,9]

Herein, a non-volatile Si racetrack resonator optical switch is demonstrated. A thin film of the PCM[10] GST, which is commonly encountered in optical and electrical data storage applications,[11–14] is used to switch the resonant frequency and Q-factor of the resonator. GST shows high optical contrast between its amorphous, covalently bonded, and crystalline, resonantly bonded, structural phases[15–18] ($n_{cryst} - n_{amorph} = 2.5$; $k_{cryst} - k_{amorph} = 1$ at $\lambda = 1.55$ μm).[19] Moreover, transitions between the two phases can take place on a sub-ns time-scale[20,21] while the resulting final state is stable for several years. These characteristics deem this material appropriate for application in reconfigurable optical circuits.

The device, shown in Fig. 1, consists of a Si racetrack resonator with a bend radius of 5 μm and a coupling region of 3 μm, on top of which a GST thin film with an area of 3×1.5 μm^2 has been deposited. A second resonator with identical dimensions but free of GST is used as a reference during the measurements. A 200 nm gap separates both resonators from a Si strip waveguide (220×440 nm^2) with grating couplers[22] at both ends, which are used to deliver light

into the device and monitor the transmitted spectrum using single-mode fibers (SMF).

The resonators, waveguides and grating couplers were fabricated on top of a silicon-on-insulator (SOI) substrate with 2 μm of buried oxide using 248 nm deep UV lithography, following a previously developed method.[23] In order to control the overlap of the mode propagating inside the resonator with the GST, a thin buffer layer (50 nm) of SiO_2 was deposited on top of the Si waveguide using plasma-enhanced chemical vapor deposition (PECVD). Subsequently, polymethylmethacrylate resist (PMMA) was spun on the SOI die and the area where the GST was to be deposited was opened using e-beam lithography. A 20 nm thick GST film was deposited into this area using radio frequency (RF) sputtering from two stoichiometric targets of GeTe and Sb_2Te_3. X-ray diffraction from other GST films, which were prepared under
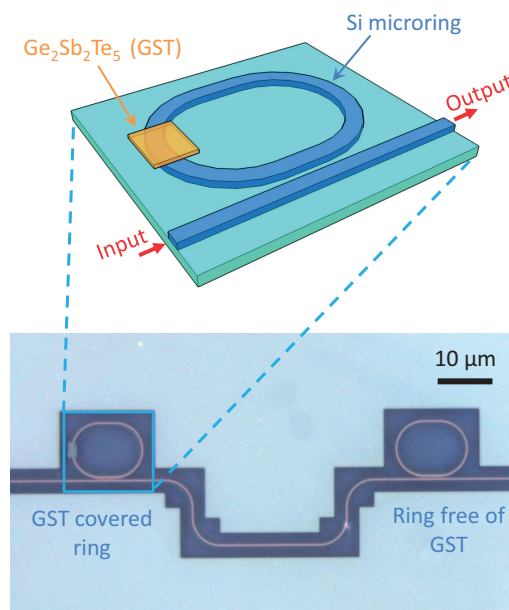

FIG. 1. Optical microscope image showing the two microrings coupled to a waveguide. The first of them (left) contains the overcladding layer of GST.

a)miquel.rude@icfo.es

TABLE I. Sputtering conditions for the $Ge_2Sb_2Te_5$ and Si_3N_4 films. The targets in all cases are 3 in. in diameter.

	$Ge_2Sb_2Te_5$		Si_3N_4	
Targets	GeTe	Sb_2Te_3	Si	
Power (type)	50 W (RF)	45 W (RF)	40 W (DC)	
Process gases	Ar		Ar	N_2
Gas flow	10 sccm		7 sccm	3 sccm
Gas pressure	3.75 mTorr		3.75 mTorr	
Time	90 s		1200 s	
Temperature	298 K		298 K	

the same conditions, confirmed the structural phase of the film to be amorphous. To avoid oxidation of this layer and achieve good thermal isolation a 20 nm film of Si_3N_4 was grown on top of the GST by reactive DC sputtering Si using a mixture of Ar and N_2 as the process gases. The sputtering conditions for these films are summarized in Table I. The sample was then put in an acetone bath for 30 min to remove the PMMA and lift off the excess material. Finally, the device was rinsed with isopropanol and blow dried.

Measurements were performed using the optical set-up shown in Fig. 2. Phase transitions in the GST layer were triggered by heating a 1 μm spot with focused laser radiation at $\lambda = 975$ nm. The electrical current driving the laser was maintained at a sub-threshold level during the experiment. Electrical pulses with tunable length and amplitude were generated in a function generator (Agilent 33220 A, 20 MHz) and amplified by a high-gain amplifier (MiniCircuits LZY-22+, 43 dB gain) before being sent to the laser through a bias-T circuit. The output optical pulses were coupled into a SMF, collimated, and focused down to a diameter of 1 μm on the sample using a 0.6 NA (50×) objective. Homogeneous illumination of the sample was achieved using a white LED and an aspheric condenser lens and cross-polarizers were used to optimize the contrast of the image. An additional short-pass infrared filter ($\lambda_{cutoff} = 950$ nm) was added to attenuate the laser beam and avoid damage to the camera. Precise alignment of the laser spot with the GST was achieved by monitoring the reflected laser spot and the sample image with a CCD camera
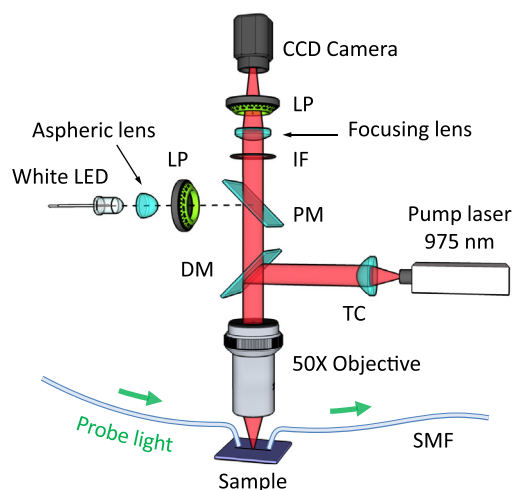

FIG. 2. Schematic of the experimental set-up (LP: Linear polarizer, DM: Dichroic mirror, IF: Infrared filter, PM: Pellicle mirror, and TC: Triplet collimator).

and then using a 3-axis stepper motorized stage to control the sample position and the focus of the 975 nm laser radiation.

Two SMF were used to couple light from a broadband ($\lambda_{min} = 1520$ nm to $\lambda_{max} = 1580$ nm) amplified spontaneous emission (ASE) source. The transmitted spectrum was recorded with an optical spectrum analyzer (OSA). Both fibers were cleaved and mounted on holders to ensure 10° incidence with the sample. Optimal coupling to and from the waveguide was achieved using two 3-axis micro-positioners. The device temperature was controlled by placing the sample on top of a thermo electrical cooler (TEC).

The laser pulse time and power for crystallization and re-amorphization of the GST film are strongly dependent on the composition, thickness, and the thermal properties of surrounding materials.[24,25] In order to confirm switching, a planar test sample with the same structure as that found on top of the resonator was fabricated on a SOI substrate. The switching parameters for this sample were then optimized by iteratively increasing the laser pulse time and power. Crystallized marks, which appear as brighter areas in the reflected image due to their higher refractive index, were repeatedly created with a laser power of 12 mW and a pulse duration of 300 ns (FWHM, 80 ns edge), while reamorphization of a crystallized area was achieved with laser pulses of 45 mW and a duration of 20 ns (FWHM, 8 ns edge). The diameter of these spots was approximately the same as the laser beam, i.e., 1 μm. The crystallization of GST is an activated process following an Arrhenius behaviour and therefore the crystallization temperature increases with heating rate,[26] changing from 455 K at a heating rate of 50 K·s^{-1} to 625 K at a heating rate of 40 000 K·s^{-1}. Herein, crystallization was achieved using 300 ns pulses; thus, the heating rate is on the order of 10^7 K·s^{-1} and the transition from the amorphous to the cubic crystalline phase is expected to occur at temperatures higher than 625 K.

A final important step before proceeding with the measurements was to analyze the effect of temperature on the transmission spectrum. Si resonators are sensitive to external variations in temperature, mainly due to the thermo-optic effect in Si.[27,28] An increase of just 1 °C (which increases n_{eff} proportionally) can manifest as a non negligible red-shift in the resonant wavelength. By scanning the temperature from 20° to 30° with the TEC, we found a value for this shift of $d\lambda/dT = 71$ pm·K^{-1}, in agreement with previous studies on similar devices.[29,30] As will be seen later, this shift is comparable to the increase in λ_{res} upon crystallization of the GST film. Therefore, the temperature during the experiment was fixed at 22 ± 0.02 °C.

Fig. 3 shows the full transmission spectrum of the device shown in Fig. 1 with the GST set in its amorphous phase. Since the device contains two resonators in series, the dips in the figure appear grouped in pairs. The left one in each pair corresponds to the resonator with GST and is modified upon phase transitions, while the right one, corresponding to the bare resonator, is used as a reference. Although the amorphous phase of GST has a small extinction coefficient ($k_{amorph} = 0.1$ at $\lambda = 1.55$ μm),[19] its presence increases the losses in the resonator, an effect which can be seen by measuring the Q factors of the bare resonator ($Q = 6528$), and the resonator covered with amorphous GST ($Q = 5656$).

Starting from this initial state, crystallization pulses with the parameters found above were used to crystallize the GST
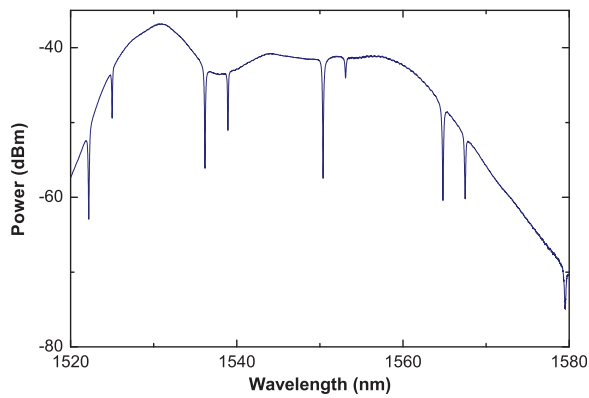
FIG. 3. Transmission spectrum between 1520 and 1580 nm. Note that the envelope of the spectrum is not flat due to ASE source.

TABLE II. Evolution of the resonator parameters during the cycle.

State	λ_{res} (nm)	n_{eff}	τ	t	Q	α (cm^{-1})
Amorphous	1550.384	2.3204	0.986	0.983	5656	7.570
33% Cryst.	1550.456	2.3205	0.977	0.983	4433	12.326
66% Cryst.	1550.492	2.3206	0.974	0.983	4115	13.983
Crystallized	1550.552	2.3207	0.968	0.983	3641	16.841
33% Ream.	1550.492	2.3206	0.972	0.983	3922	15.145
66% Ream.	1550.396	2.3205	0.974	0.983	4051	14.454
Reamorphized	1550.372	2.3204	0.986	0.983	5411	7.160

film. Due to the GST area ($3 \times 1.5 \, \mu m^2$) being larger than the focused laser spot ($1 \, \mu m$), it was necessary to move ($1 \, \mu m$ steps) the laser across the area and repeatedly apply the crystallization pulse until the complete area of GST was crystallized. In actuality, this could be achieved with just 3 shots along the axis waveguide (Fig. 4(a)). The same process was repeated using reamorphization pulses to recover the transmissivity at $\lambda = 1.55 \, \mu m$, thus completing a full cycle (Fig. 4(b)).

The effect of the structural phase transitions on the device transmission was analyzed using the power transfer function of a racetrack resonator, which is given by[31]

$$\frac{P_{\text{out}}}{P_{\text{in}}} = \frac{\tau^2 - 2t\tau \cos \phi + t^2}{1 - 2t\tau \cos \phi + t^2\tau^2}. \quad (1)$$

Here, τ is the decay constant of the optical mode inside the resonator, which determines the losses $\alpha = -2 \log \tau/L$, t is the electric field transmission coefficient at the coupler, and $\phi = \frac{2\pi}{\lambda} L n_{\text{eff}}$ is the phase shift after one round trip. By fitting the data in Fig. 4 to Eq. (1), it was possible to determine the evolution of these values during one crystallization/reamorphization cycle (see Table II).

One can see that the optical properties of the final amorphous state are quite similar to those of the initial one, with maximum differences in the values lying around 5%, indicating that the switch performance is robust and reversible. If

one considers the out-of-equilibrium nature of the sputter deposition process, then small differences between the optical properties of the as-deposited amorphous state and the laser reamorphized state are to be expected. These differences have been confirmed to remain below 8.5%, the standard for optical recording applications, for more than 5×10^5 switching cycles,[32] and similar performance is expected for the GST on top of the resonator. Table II also shows a clear effect of the amorphous to crystalline phase transition on the transmission. The increase in the refractive index of GST upon crystallization increases the averaged out effective refractive index of the ring by 0.0003, producing a red shift of $\lambda_{\text{cryst}} - \lambda_{\text{amorph}} = 168$ pm, while the higher absorption coefficient increases the losses α in the resonator (thus decreasing τ and the Q factor). As expected, the transmission coefficient t, which only depends on the coupling efficiency between the waveguide and the resonator, remains the same in all cases. Finally, labelling the amorphous phase as the "off" state and the crystalline one as the "on" state, the combination of both effects produces a modulation of 12.36 dB at $\lambda = 1550.384$ nm. In this case, the insertion loss in the "on" state is -2.5 dB.

All of the aforementioned measurements were static, but it is also interesting to investigate the time response of the device. For this purpose, the ASE source was replaced by a tunable laser (HP 8168F) and the OSA by a fast photodiode (ThorLabs PDA8GS, < 1 ns rise time). In this way, the laser was tuned at the respective λ_{res} of the amorphous/crystalline state and using 0.4 mW of optical power the response of the device during one crystallization/reamorphization pulse was monitored by an oscilloscope (see Fig. 5).
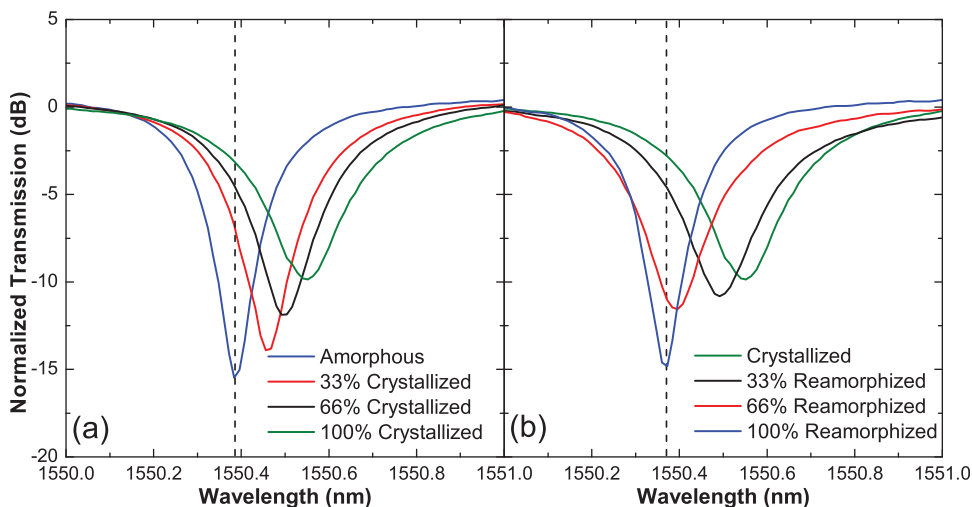

FIG. 4. Evolution of the spectrum during crystallization (a) and reamorphization (b) of the $1.5 \times 3 \, \mu m^2$ GST area.

The dynamics of this response can be understood if one considers the light induced phase transition of the GST film as well as thermal effects in the Si resonator following light absorption in the GST. Note that in this experiment, the former can be generated by the pump beam while the latter by both the pump and probe laser. Let us first consider the Si resonator without GST. In this case, the above effects are not present (absence of PCM). In addition, the thermo-optic effect due to only Si absorption is experimentally confirmed to be negligible. For the Si resonator with GST, when the switching laser pulse reaches and is absorbed by the amorphous GST, it heats it up, thus starting to induce crystallization, and at the same time causing a red-shift of the resonance (observed as an increase in transmission in Fig. 5(a-ii)). As a consequence of this red-shift, the resonating optical power of the probe in the resonator is reduced, as well as the heating due to its absorption in the GST. Therefore, a blue-shift of the resonance occurs, causing a drop in transmission (Fig. 5(a-iii)). This blue-shift once again increases the optical power resonating inside, and therefore, a new red-shift occurs, until, after approximately $5 \mu s$, all the induced effects have reached a steady state condition (Fig. 5(a-iv)). When the initial phase is crystalline the dynamics are similar except that they are generated with a shorter pump pulse (20 ns), and that the final resonant wavelength is shorter than the probe one (Figs. 5(b-v)–5(b-viii)).

In conclusion, we have demonstrated that the optical contrast of PCMs thin films can be used to reversibly tune the resonances in a Si racetrack resonator between two well-defined states. Using this effect, which is triggered by means of optical pulses from an infrared laser diode, we have achieved an optical switch with an on/off ratio higher than 12 dB and response times of approximately $5 \mu s$, operating at
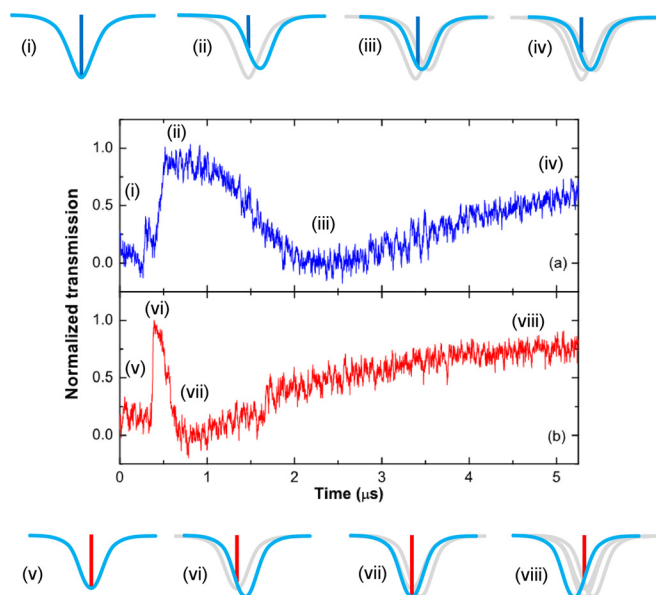
telecommunication wavelengths. By using heat-sinking structures with high thermal conductivity the time response of the device could be enhanced and limited only by the phase transition times of PCMs, while optimization of the microring and GST geometries could reduce the insertion loss well below 1 dB.

[1] Q. F. Xu, B. Schmidt, S. Pradhan, and M. Lipson, Nature **435**(7040), 325 (2005).

[2] G. T. Reed, G. Mashanovich, F. Y. Gardes, and D. J. Thompson, Nature Photon. **4**(8), 518 (2010).

[3] M. Liu, X. B. Yin, E. Ulin-Avila, B. S. Jeng, T. Zentgraf, L. Ju, F. Wang, and X. Zhang, Nature **474**(7349), 64 (2011).

[4] Q. F. Xu and M. Lipson, Opt. Express **15**(3), 924 (2007).

[5] V. R. Almeida, C. A. Barrios, R. R. Panepucci, and M. Lipson, Nature **431**, 1081 (2004).

[6] S. Xiao, M. H. Khan, H. Shen, and M. Qi, Opt. Express **15**, 14765 (2007).

[7] Q. F. Xu, B. Schmidt, J. Shakya, and M. Lipson, Opt. Express **14**(20), 9431 (2006).

[8] J. Pello, J. J. G. M. van der Tol, M. Rudé, R. E. Simpson, S. Keyvaninia, G. Roelkens, M. K. Smit, and V. Pruneri, in 16th European Conference on Integrated Optics and Technical Exhibition (ECIO), Barcelona, Spain, 2012.

[9] W. H. P. Pernice and H. Bhaskaran, Appl. Phys. Lett. **101**, 171101 (2012).

[10] D. Lencer, M. Salinga, B. Grabowski, T. Hickel, J. Neugebauer, and M. Wuttig, Nature Mater. **7**, 972 (2008).

[11] M. Wuttig and N. Yamada, Nature Mater. **6**, 824 (2007).

[12] A. V. Kolobov, P. Fons, A. I. Frenkel, A. L. Ankudinov, J. Tominaga, and T. Uruga, Nature Mater. **3**, 703 (2004).

[13] M. H. R. Lankhorst, B. W. Ketelaars, and R. A. M. Wolters, Nature Mater. **4**, 347 (2005).

[14] R. E. Simpson, P. Fons, A. V. Kolobov, T. Fukaya, M. Krbal, T. Yagi, and J. Tominaga, Nature Nanotechnol. **6**, 501 (2011).

[15] K. Shportko, S. Kremers, M. Woda, D. Lencer, J. Robertson, and M. Wuttig, Nature Mater. **7**, 653 (2008).

[16] B. Huang and J. Robertson, Phys. Rev. B **81**(8), 081204 (2010).

[17] W. Welnic, S. Botti, L. Reining, and M. Wuttig, Phys. Rev. Lett. **98**, 236403 (2007).

[18] J. Robertson, Thin Solid Films **515**, 7538 (2007).

[19] *Various, Phase Change Materials: Science and Applications*, edited by M. Wuttig and S. Raoux (Springer-Verlag, New York, 2008), p. 178.

[20] J. Hegedüs and S. R. Elliott, Nature Mater. **7**, 399 (2008).

[21] D. Loke, T. H. Lee, W. J. Wang, L. P. Shi, R. Zhao, Y. C. yeo, T. C. Chong, and S. R. Elliott, Science **336**(6088), 1566 (2012).

[22] G. Roelkens, D. Vermeulen, F. van Laere, S. Selvaraja, S. Scheerlink, D. Taillaert, W. Bogaerts, P. Dumon, D. van Thourhout, and R. Baets, J. Nanosci. Nanotechnol. **10**(3), 1551 (2010).

[23] P. Dumon, W. Bogaerts, V. Wiaux, J. Wouters, S. Beckx, J. Van Campenhout, D. Taillaert, B. Luyssaert, P. Bienstman, D. Van Thourhout, and R. Baets, IEEE Photon. Technol. Lett. **16**(5), 1328 (2004).

[24] R. E. Simpson, M. Krbal, P. Fons, A. V. Kolobov, J. Tominaga, T. Uruga, and H. Tanida, Nano Lett. **10**(2), 414 (2010).

[25] X. Wei, L. Shi, T. C. Chong, R. Zhao, and H. K. Lee, Jpn. J. Appl. Phys., Part 1 **46**, 2211 (2007).

[26] J. Orava, A. L. Greer, B. Gholipour, D. W. Hewak, and C. E. Smith, Nature Mater. **11**, 279 (2012).

[27] F. G. D. Corte, M. E. Montefusco, L. Moretti, I. Rendina, and G. Cocorullo, J. Appl. Phys. **88**(12), 7115 (2000).

[28] G. Cocorullo, F. G. D. Corte, I. Rendina, and P. M. Sarro, Sens. Actuators, A **71**(1–2), 19 (1998).

[29] J. Teng, P. Dumon, W. Bogaerts, H. B. Zhang, X. G. Jian, X. Y. Han, M. S. Zhao, G. Morthier, and R. Baets, Opt. Express **17**(17), 14627 (2009).

[30] W. N. Ye, J. Michel, and L. C. Kimerling, IEEE Photon. Technol. Lett. **20**(11), 885 (2008).

[31] W. Bogaerts, P. de Heyn, T. van Vaerenbergh, K. de Vos, S. K. Selvaraja, T. Claes, P. Dumon, P. Bienstman, D. Van Thourhout, and R. Baets, Laser Photonics Rev. **6**(1), 47 (2012).

[32] *Phase Change Materials: Science and Applications*, edited by M. Wuttig and S. Raoux (Springer Verlag, New York, 2008), p. 212.

FIG. 5. Time response of the device during (a) a crystallization pulse ($\lambda_{probe} = 1550.384$ nm) and (b) a reamorphization pulse ($\lambda_{probe} = 1550.552$ nm). Increasing values in the graph indicate higher transmission at that wavelength. Diagrams (i)–(iv) and (v)–(viii) represent the expected change in the device spectrum with respect to λ_{probe} at different moments during the crystallization and the reamorphization process, respectively.